arXiv:1710.09127v1 [cond-mat.mes-hall] 25 Oct 2017

Design of an optimized MoS_2-based highly sensitive near-infrared surface plasmon resonance imaging biosensor

YI XU,[1] LIN WU,[2] AND LAY KEE ANG[1,*]

[1] *SUTD-MIT International Design Center, Singapore University of Technology and Design, Singapore 487372*

[2] *Institute of High Performance Computing, Agency for Science, Technology, and Research (A*STAR), 1 Fusionopolis Way, #16-16 Connexis, Singapore 138632*

[*] *ricky_ang@sutd.edu.sg*

Abstract: A surface plasmon resonance imaging biosensor based on MoS_2 deposited on Aluminium substrate is designed for high imaging sensitivity and detection accuracy. The proposed biosensor exhibits better performance than graphene-based biosensor in the near-infrared regime. A high imaging sensitivity of more than 970 RIU^{-1} is obtained at the wavelength of 1540 nm. The effect of aluminium thickness, number of MoS_2 layers and the refractive index of sensing layer are investigated to obtain an optimized design for high sensor performance. In addition, the sensor performance comparison of MoS_2 and other two-dimensional transition metal dichalcogenide materials based biosensor in the near-infrared regime are also presented. The designed MoS_2 mediated surface plasmon resonance imaging biosensor could provide potential applications in surface plasmon resonance imaging detection of multiple biomolecular interactions simultaneously.

© 2024 Optical Society of America under the terms of the OSA Open Access Publishing Agreement

OCIS codes: (240.6680) Surface plasmons; (280.4788) Optical sensing and sensors; (280.1415) Biological sensing and sensors.

References and links

1. J. Homola, S. S. Yee, and G. Gauglitz, "Surface plasmon resonance sensors: review," Sens. Actuators B Chem. **54**(1-2), 3–15 (1999).
2. J. Homola, "Surface plasmon resonance sensors for detection of chemical and biological species," Chem. Rev. **108**(2), 462–493 (2008).
3. X. Fan, I. M. White, S. I. Shopova, H. Zhu, J. D. Suter, and Y. Sun, "Sensitive optical biosensors for unlabeled targets: A review," Anal. Chim. Acta **620**(1-2), 8–26 (2008).
4. E. Wijaya, C. Lenaerts, S. Maricot, J. Hastanin, S. Habraken, J.-P. Vilcot, R. Boukherroub, and S. Szunerits, "Surface plasmon resonance-based biosensors: From the development of different spr structures to novel surface functionalization strategies," Curr. Op. Sol. St. M. **15**(5), 208–224 (2011).
5. E. Kretschmann and H. Raether, "Notizen: radiative decay of non radiative surface plasmons excited by light," Z. Naturforsch. A **23**(12), 2135–2136 (1968).
6. A. W. Wark, H. J. Lee, and R. M. Corn, "Long-range surface plasmon resonance imaging for bioaffinity sensors," Anal. Chem. **77**(13), 3904–3907 (2005).
7. H. J. Lee, D. Nedelkov, and R. M. Corn, "Surface plasmon resonance imaging measurements of antibody arrays for the multiplexed detection of low molecular weight protein biomarkers," Anal. Chem. **78**(18), 6504–6510 (2006).
8. Y. Zeng, R. Hu, L. Wang, D. Gu, J. He, S.-Y. Wu, H.-P. Ho, X. Li, J. Qu, B. Z. Gao, Y. Shao, "Recent advances in surface plasmon resonance imaging: detection speed, sensitivity, and portability," Nanophotonics **6**(5), 1017–1030 (2017).
9. S. H. Choi and K. M. Byun, "Investigation on an application of silver substrates for sensitive surface plasmon resonance imaging detection," J. Opt. Soc. Am. A **27**(10), 2229–2236 (2010).
10. C. L. Wong and M. Olivo, "Surface plasmon resonance imaging sensors: a review," Plasmonics **9**(4), 809–824 (2014).
11. M. W. Knight, N. S. King, L. Liu, H. O. Everitt, P. Nordlander, and N. J. Halas, "Aluminum for plasmonics," ACS Nano **8**(1), 834–840 (2013).
12. N. S. King, L. Liu, X. Yang, B. Cerjan, H. O. Everitt, P. Nordlander, and N. J. Halas, "Fano resonant aluminum nanoclusters for plasmonic colorimetric sensing," ACS Nano **9**(11), 10628–10636 (2015).
13. W. Li, K. Ren, and J. Zhou, "Aluminum-based localized surface plasmon resonance for biosensing," TrAC Trends Anal. Chem. **80**, 486–494 (2016).

14. P. K. Maharana, T. Srivastava, and R. Jha, "Ultrasensitive plasmonic imaging sensor based on graphene and silicon," IEEE Photon. Technol. Lett. **25**(2), 122–125 (2013).
15. P. K. Maharana, T. Srivastava, and R. Jha, "On the performance of highly sensitive and accurate graphene-on-aluminum and silicon-based spr biosensor for visible and near infrared," Plasmonics **9**(5), 1113–1120 (2014).
16. S. H. Choi, Y. L. Kim, and K. M. Byun, "Graphene-on-silver substrates for sensitive surface plasmon resonance imaging biosensors," Opt. Express **19**(2), 458–466 (2011).
17. L. Wu, H. Chu, W. Koh, and E. Li, "Highly sensitive graphene biosensors based on surface plasmon resonance," Opt. Express **18**(14), 14395–14400 (2010).
18. A. C. Ferrari, F. Bonaccorso, V. Fal'Ko, K. S. Novoselov, S. Roche, P. Bøggild, S. Borini, F. H. Koppens, V. Palermo, N. Pugno, J. A. Garrido, R. Sordan, A. Bianco, L. Ballerini, M. Prato, E. Lidorikis, J. Kivioja, C. Marinelli, T. Ryhänen, A. Morpurgo, J. N. Coleman, V. Nicolosi, L. Colombo, A. Fert, M. Garcia-Hernandez, A. Bachtold, G. F. Schneider, F. Guinea, C. Dekker, M. Barbone, Z. Sun, C. Galiotis, A. N. Grigorenko, G. Konstantatos, A. Kis, M. Katsnelson, L. Vandersypen, A. Loiseau, V. Morandi, D. Neumaier, E. Treossi, V. Pellegrini, M. Polini, A. Tredicucci, G. M. Williams, B. H. Hong, J. H. Ahn, J. M. Kim, H. Zirath, B. J. van Wees, H. van der Zant, L. Occhipinti, A. Di Matteo, I. A. Kinloch, T. Seyller, E. Quesnel, X. Feng, K. Teo, N. Rupesinghe, P. Hakonen, S. R. T. Neil, Q. Tannock, T. Löfwander, and J. Kinaret, "Science and technology roadmap for graphene, related two-dimensional crystals, and hybrid systems," Nanoscale **7**(11), 4598–4810 (2015).
19. F. K. Perkins, A. L. Friedman, E. Cobas, P. Campbell, G. Jernigan, and B. T. Jonker, "Chemical vapor sensing with monolayer mos2," Nano Lett. **13**(2), 668–673 (2013).
20. S. Zeng, S. Hu, J. Xia, T. Anderson, X.-Q. Dinh, X.-M. Meng, P. Coquet, and K.-T. Yong, "Graphene–mos2 hybrid nanostructures enhanced surface plasmon resonance biosensors," Sens. Actuators B Chem. **207**, 801–810 (2015).
21. A. K. Mishra, S. K. Mishra, and R. K. Verma, "Graphene and beyond graphene mos2: a new window in surface-plasmon-resonance-based fiber optic sensing," J. Phys. Chem. C **120**(5), 2893–2900 (2016).
22. C. Rao, K. Gopalakrishnan, and U. Maitra, "Comparative study of potential applications of graphene, mos2, and other two-dimensional materials in energy devices, sensors, and related areas," ACS Appl. Mater. Interfaces **7**(15), 7809–7832 (2015).
23. Q. Ouyang, S. Zeng, L. Jiang, J. Qu, X.-Q. Dinh, J. Qian, S. He, P. Coquet, and K.-T. Yong, "Two-dimensional transition metal dichalcogenide enhanced phase-sensitive plasmonic biosensors: Theoretical insight," J. Phys. Chem. C **121**(11), 6282–6289 (2017).
24. Q. Ouyang, S. Zeng, L. Jiang, L. Hong, G. Xu, X.-Q. Dinh, J. Qian, S. He, J. Qu, P. Coquet, K.-T. Yong, "Sensitivity enhancement of transition metal dichalcogenides/silicon nanostructure-based surface plasmon resonance biosensor," Sci. Rep. **6**, 28190 (2016).
25. K. Kalantar-zadeh and J. Z. Ou, "Biosensors based on two-dimensional mos2," ACS Sens. **1**(1), 5–16 (2015).
26. D. Sarkar, W. Liu, X. Xie, A. C. Anselmo, S. Mitragotri, and K. Banerjee, "Mos2 field-effect transistor for next-generation label-free biosensors," ACS Nano **8**(4), 3992–4003 (2014).
27. J. Lee, P. Dak, Y. Lee, H. Park, W. Choi, M. A. Alam, and S. Kim, "Two-dimensional layered mos2 biosensors enable highly sensitive detection of biomolecules," Sci. Rep. **4**, 7352 (2014).
28. O. Lopez-Sanchez, D. Lembke, M. Kayci, A. Radenovic, and A. Kis, "Ultrasensitive photodetectors based on monolayer mos2," Nat. Nanotechnol. **8**(7), 497–501 (2013).
29. K. Roy, M. Padmanabhan, S. Goswami, T. P. Sai, G. Ramalingam, S. Raghavan, and A. Ghosh, "Graphene-mos2 hybrid structures for multifunctional photoresponsive memory devices," Nat. Nanotechnol. **8**(11), 826–830 (2013).
30. K. F. Mak, C. Lee, J. Hone, J. Shan, and T. F. Heinz, "Atomically thin mos2: a new direct-gap semiconductor," Phys. Rev. Lett. **105**, 136805 (2010).
31. D. Lembke, S. Bertolazzi, and A. Kis, "Single-layer mos2 electronics," Acc. Chem. Res. **48**(1), 100–110 (2015).
32. Q. H. Wang, K. Kalantar-Zadeh, A. Kis, J. N. Coleman, and M. S. Strano, "Electronics and optoelectronics of two-dimensional transition metal dichalcogenides," Nat. Nanotechnol. **7**(11), 699–712 (2012).
33. A. B. Farimani, K. Min, and N. R. Aluru, "DNA base detection using a single-layer mos2," ACS Nano **8**(8), 7914–7922 (2014).
34. P. K. Maharana and R. Jha, "Chalcogenide prism and graphene multilayer based surface plasmon resonance affinity biosensor for high performance," Sens. Actuators B Chem. **169**, 161–166 (2012).
35. M. Yamamoto, "Surface plasmon resonance (spr) theory: tutorial," Review of Polarography **48**, 209–237 (2002).
36. J. Weber, V. Calado, and M. Van de Sanden, "Optical constants of graphene measured by spectroscopic ellipsometry," Appl. Phys. Lett. **97**(9), 091904 (2010).
37. S. Yang, C. Jiang, and S.-H. Wei, "Gas sensing in 2D materials," Appl. Phys. Rev. **4**(2), 021304 (2017).
38. G. Yang, C. Zhu, D. Du, J. Zhu, and Y. Lin, "Graphene-like two-dimensional layered nanomaterials: applications in biosensors and nanomedicine," Nanoscale **7**(34), 14217–14231 (2015).

1. Introduction

Surface plasmon resonance (SPR), in which surface plasmon waves (SPWs) are excited at the metal-dielectric interface, has been widely employed in the sensing applications over the last few decades [1–4]. Many optical structures have been proposed to excite SPWs [1, 2], like

prism-coupling, waveguide-coupling and grating-coupling. A typical SPW excitation structure is the Kretschmann configuration [5], where a thin metal film is coated over the base of a prism. The SPWs are excited by a p-polarized light when the propagation constant of the incident light along the metal-dielectric interface matches the propagation constant of SPW [1]. The excitation of SPWs depends on the refractive index (RI) of dielectric medium that in contact with the metal thin film. Therefore, SPR can be used to detect the variation of ambient RI. One of the widely used SPR sensing techniques is the angle interrogation scheme, which is a sensitive and robust detection method for SPR sensors. In this approach, a p-polarized monochromatic light is employed to excite SPWs at the metal-dielectric interface, and the reflectance is monitored as a function of the incident angle. However, one limitation of this scheme is its inability to measure diverse sets of samples at a time. SPR imaging sensors [6–10], measure numerous samples in a parallel manner, have been proposed and demonstrated to overcome this limitation. Noted for a SPR imaging sensor, the spatial variations in reflectivity are measured at a fixed incident angle (i.e., no moving parts) due to the ambient RI changes.

Noble metals, like gold and silver, are usually employed to excite SPWs in SPR sensors. However, gold-based SPR sensor shows a broader SPR curve which degrades the detection accuracy. In contrast, aluminium (Al) is a promising material for plasmonics application [11–15] not only because its narrow SPR curve, tunable plasmon resonant from visible to ultraviolet regime, but also for low cost. However, Al is prone to oxidation which will decrease the sensor performances. Recently, two-dimensional (2D) nanomaterials, like graphene, have been proposed to inhibit the oxidation of Al thin film in SPR sensors [14, 15]. Although coating Al thin film with graphene layers will decrease the sensor sensitivity, the protected SPR sensor can still obtain an exceptionally high sensitivity due to the atomic thickness of the 2D nonmaterial.

In addition to the graphene-based SPR sensor [14–18], 2D transition metal dichalcogenides (TMDCs) such as Molybdenum disulfide (MoS_2) have also been widely employed in sensing applications [19–27]. Compared with graphene, monolayer MoS_2 has a higher optical absorption efficiency (~5%) [28], which provides promising applications in various optoelectronic nanodevices, such as photodetectors with a high responsivity of $5 \times 10^8 \mathrm{AW}^{-1}$ [29]. The nonzero tunable band gap of MoS_2 [30] makes it an attractive candidate for future nanoelectronic devices as well as biosensors [31, 32]. For example, the nonzero bandgap of MoS_2 can be utilized to fabricate an ultrasensitive field-effect transistor biosensor based on MoS_2, while the zero bandgap in graphene limits the sensitivity of graphene-based field-effect transistor biosensor [26]. In addition, the hydrophobic nature of MoS_2 allows it to be used in biosensors as a recognition layer which exhibits high affinity to biomolecules absorption [27, 33]. All these exciting properties make MoS_2 a highly potential candidate for biosensing applications. Taking the advantages of SPR imaging sensor, Al and MoS_2, a highly sensitive and accurate SPR imaging biosensor based on MoS_2 deposited on Al thin film has been designed in this paper. The MoS_2 layer in our designed configuration serves two purposes, as the protective layer of Al thin film and as the recognition layer to capture the biomolecules. We first compared the sensor performance of our design to the graphene-based SPR imaging sensor in the visible and near-infrared regime, which shows that MoS_2-based sensor has a better performance in the near-infrared region. By focusing in the near-infrared regime, we have studied various designed parameters in details in order to obtain an optimized performance including the effects of multiple layers of MoS_2, thickness of the Al film, and RI of the sensing layer. In addition, the performances of other 2D TMDCs based biosensors have also compared at the end.

2. Theoretical Model

The Kretschmann configuration is employed to design our proposed biosensor structure, as shown in Fig. 1. In the proposed design, MoS_2 coated Al thin film is attached to a chalcogenide (2S2G) glass prism, which is a promising candidate for the design of SPR sensor due to its broad

operating window (from visible to near-infrared regime) and high RI. A p-polarized light with a fixed wavelength is incident at one side of the prism with a fixed incident angle, while the reflected light is collected on the other side.

The wavelength-dependent RI of the 2S2G prism is given by [34]:

$$n_{2S2G} = 2.24047 + \frac{2.693 \times 10^{-2}}{\lambda^2} + \frac{9.08 \times 10^{-3}}{\lambda^4}, \tag{1}$$

where the wavelength λ is given in μm. The RI of Al is given by

$$n_{Al} = \left(1 - \frac{\lambda^2 \lambda_c}{\lambda_p^2(\lambda_c + i\lambda)}\right)^{1/2}, \tag{2}$$

according to the Drude-Lorentz model [15]. Here, λ_p (=1.0657×10^{-7} m) and λ_c (=2.4511×10^{-5} m) is the plasma wavelength and collision wavelength of Al, respectively. The thickness of monolayer MoS_2 is 0.65 nm, and its RI in visible and near-infrared region is shown in Table 1 [23]. The RI of the sensing layer is initially set to $n_s = 1.330$.

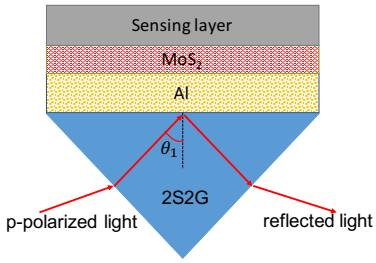


Fig. 1. Schematic of MoS_2-based SPR imaging sensor.

Table 1. RI of Monolayer MoS_2 in the Near-Infrared Region [23]

wavelength	RI
λ=633 nm	$5.0805 + i1.1732$
λ=785 nm	$4.6348 + i0.1163$
λ=904 nm	$4.7261 + i0.1346$
λ=1150 nm	$4.4317 + i0.0721$
λ=1540 nm	$4.2374 + i0.0325$

To obtain the reflectance of the sensor configuration, a generalized N-layer model [35] was employed, and the reflectance R for the p-polarized incident light is given by

$$R = \left| \frac{(M_{11} + M_{12}q_N)q_1 - (M_{21} + M_{22}q_N)}{(M_{11} + M_{12}q_N)q_1 + (M_{21} + M_{22}q_N)} \right|^2, \tag{3}$$

with

$$M = \begin{bmatrix} M_{11} & M_{12} \\ M_{21} & M_{22} \end{bmatrix} = \prod_{k=2}^{N-1} M_k, \tag{4}$$

and

$$M_k = \begin{bmatrix} \cos\beta_k & -i(\sin\beta_k)/q_k \\ -iq_k \sin\beta_k & \cos\beta_k \end{bmatrix}. \tag{5}$$

We denote

$$\beta_k = \frac{2\pi d_k}{\lambda}\left(n_k^2 - n_1^2 \sin^2\theta_1\right), \tag{6}$$

and

$$q_k = \frac{\left(n_k^2 - n_1^2 \sin^2\theta_1\right)^{1/2}}{n_k^2}, \tag{7}$$

where n_k and d_k are respectively the RI and thickness of the kth layer with $k = 2$ to $N-1$. The first layer ($k = 1$) is the 2S2G prism, and the last layer ($k = N$) is the sensing layer. θ_1 is the incident angle at the prism-Al interface, and λ is the wavelength of the p-polarized incident light.

A variation of the sensing layer RI (n_s) will cause a change in the reflectance R, and the imaging sensitivity of the SPR sensor is defined as

$$S = \frac{dR}{dn_s}, \tag{8}$$

where the reflectance R is given in Eq. (3). Besides the imaging sensitivity, another important parameter for the sensor performance is the full width at half maximum (FWHM) of the reflectance curve, which describes the detection accuracy of the sensor. To achieve a excellent performance imaging sensor, we note that the sensor should exhibits high imaging sensitivity and low FWHM (i.e., high detection accuracy).

3. Results and discussion

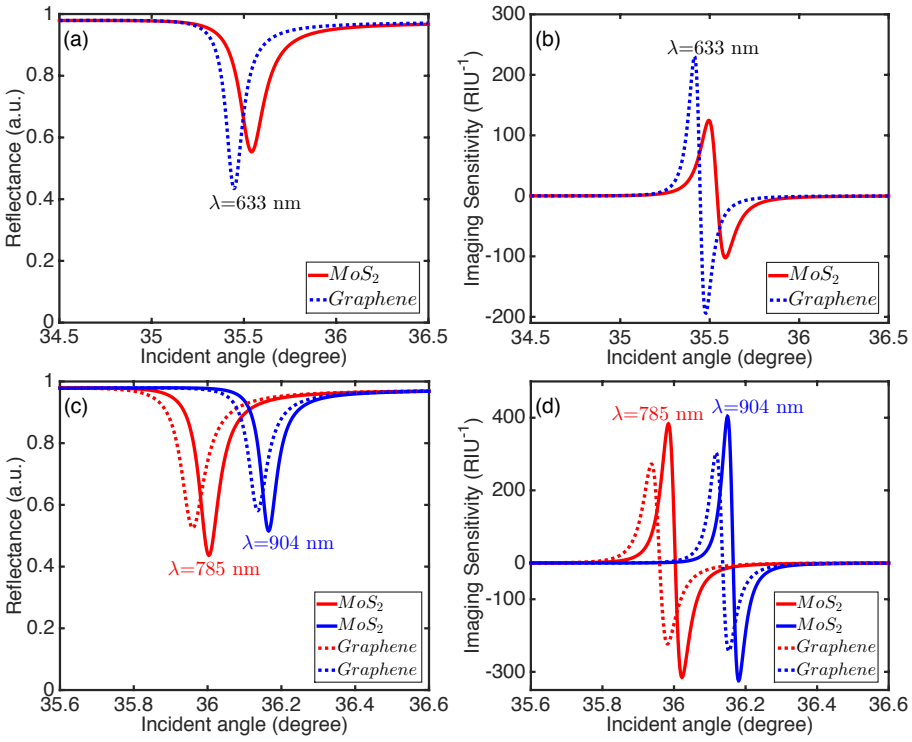


Fig. 2. Reflectance (a)(c) and imaging sensitivity (b)(d) for monolayer MoS_2 and graphene-based sensor at λ = 633 nm, 785 nm and 904 nm. The Al thickness is 50 nm.

The reflectance and imaging sensitivity for two sensors: a monolayer MoS_2-based sensor and graphene-based sensor, both deposited on a 50 nm thick Al film are shown in Fig. 2 for both visible (λ = 633 nm) and near-infrared (λ = 785 nm and 904 nm) wavelengths. The RI of graphene in the visible and near-infrared region is taken from Ref. [36]. In the visible region (λ = 633 nm), graphene-based sensor shows a narrow SPR curve in comparison with that of MoS_2-based sensor (0.1082^o vs. 0.1591^o), as shown in Fig. 2(a). For the imaging sensitivity, it is found that the sensitivity exhibits a positive peak as well as a negative peak (see Fig. 2(b) and (d)). We only considered the positive peak imaging sensitivity since its magnitude is higher than that of negative peak (see Fig. 2(b) and (d)). In the following, the imaging sensitivity means the positive peak imaging sensitivity. The imaging sensitivity of graphene-based sensor (230.4 RIU^{-1}) is higher than the sensitivity for MoS_2-based imaging sensor (124.8 RIU^{-1}) at λ = 633 nm. However, at the near-infrared region (λ = 785 nm and 904 nm), the imaging sensitivity of MoS_2-based sensor is higher than that of graphene-based sensor (see Fig. 2(d) and Table 2). The FWHM of MoS_2-based sensor in the near-infrared region is smaller than that of graphene-based sensor (see Table 2). Thus the findings of high imaging sensitivity and low FWHM have indicated that MoS_2 based sensor has better performance than graphene-based sensor in the near-infrared region. The trends also indicates its better performance may be extended to even longer wavelengths, and thus we will focus on three longer wavelengths (785 nm, 1150 nm and 1540 nm) in the optical near-infrared regime in the subsequent studies.

Table 2. Comparison of sensor performances for monolayer MoS_2- and graphene-based sensor in the visible and near-Infrared Region.

	Imaging Sensitivity (RIU^{-1})		FWHM (degree)	
wavelength	MoS_2-based	graphene-based	MoS_2-based	graphene-based
λ = 633 nm	124.8	230.4	0.1591	0.1082
λ = 785 nm	383.4	272.7	0.0657	0.0772
λ = 904 nm	403.9	303.6	0.0538	0.0613

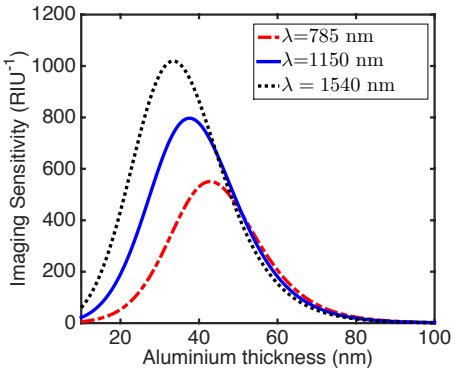


Fig. 3. Imaging sensitivity as a function of the Al thickness without MoS_2 coated.

Before investigating the sensor performance of MoS_2-based biosensor at longer wavelength, we first optimize the Al thickness since the thickness of plasmonics supporting material is an important parameter for the SPR sensor performance. The imaging sensitivity as a function of the Al thickness (without coated MoS_2) at wavelengths λ = 785 nm, 1150 nm and 1540 nm is shown in Fig. 3. It can be seen from Fig. 3 that the optimized Al thickness decreases with the increasing wavelength. Here, we consider the optimized Al thickness is 38 nm, at which at least

90% of the maximum imaging sensitivity's value can be obtained for all three wavelengths.

The effect of multiple MoS_2 layers on the reflectance and sensor performance at three different wavelengths is shown in Fig. 4. It is found that the resonance curves become shallower and broader (larger FWHM, see Fig. 4(d)) with the number of MoS_2 layers increases, which is a result of the increased surface plasmon damping. For example, with monolayer MoS_2 coated sensor, the FWHM is 0.105^o at $\lambda = 785$ nm, while FWHM is 0.0532^o at $\lambda = 1150$ nm and 0.0343^o at $\lambda = 1540$ nm. When the Al thin film is coated with 20 layers MoS_2, the FWHM becomes quite large at $\lambda = 785$ nm (1.249^o), while the FWHM at longer wavelength is still small (0.1791^o at $\lambda = 1150$ nm and 0.0755^o at $\lambda = 1540$ nm). In addition, the resonance angle increases with the number of MoS_2 layers. For the imaging sensitivity, it decreases with the increasing number of MoS_2 layers (see Fig. 4(d)) due to the increased loss within the MoS_2 layers. As mentioned before, Al is susceptible to oxidation which deceases the sensor performances, whereas MoS_2 layers deposited on Al thin film can be utilized to inhibit the oxidation of Al. Although coating with MoS_2 decreases the imaging sensitivity, the designed biosensors with monolayer or bilayer MoS_2 can still provide exceptional sensitivities. For monolayer MoS_2-based sensor, the imaging sensitivity is 442 RIU^{-1} at $\lambda = 785$ nm, 745.8 RIU^{-1} at $\lambda = 1150$ nm and 895.6 RIU^{-1} at $\lambda = 1540$ nm. It is noted that the proposed biosensor provides a relative high sensitivity of 397.8 RIU^{-1} at $\lambda = 1540$ nm with 20 layers MoS_2, while it is only 36.96 RIU^{-1} at $\lambda = 785$ nm. Higher sensitivity and smaller FWHM are obtained at higher wavelength, which is consistent with the results shown in Fig. 2.

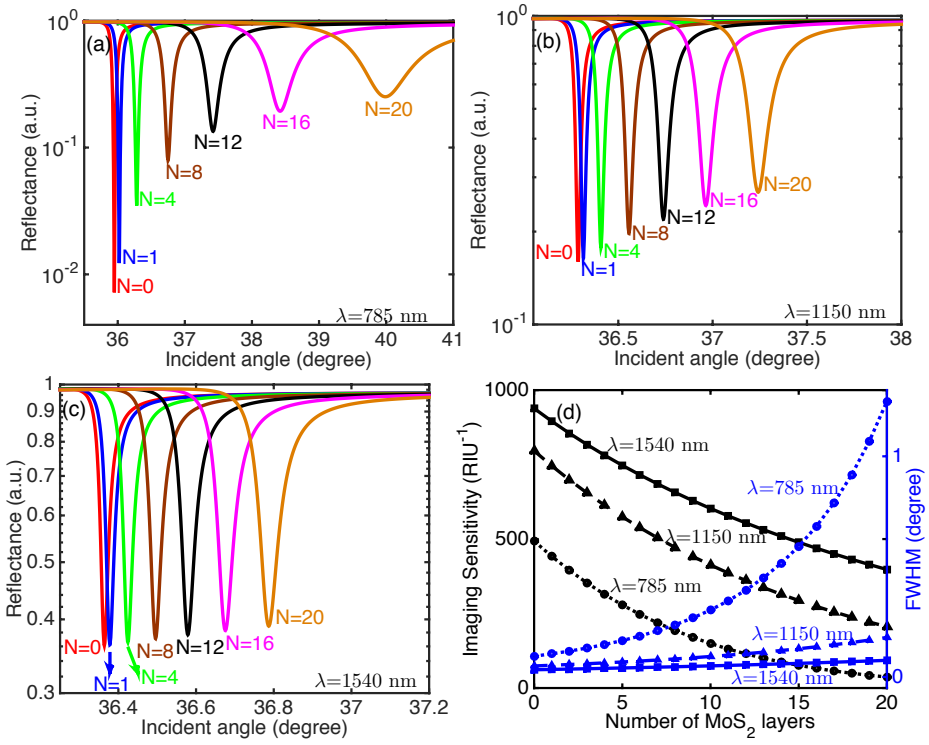


Fig. 4. Reflectance as a function of incident angle for multiple MoS_2-based SPR imaging sensor at wavelength (a) $\lambda = 785$ nm, (b) $\lambda = 1150$ nm and (c) $\lambda = 1540$ nm. (d) Imaging sensitivity and FWHM for SPR imaging sensor with multiple MoS_2 layers at different wavelengths. The Al thickness is 38 nm.

To optimize the design of MoS_2-on-Al SPR imaging sensor, Fig. 5 shows the imaging sensitivity

as a function of the number of MoS_2 layers and Al thickness at three different wavelengths: 785 nm, 1150 nm and 1540 nm. For monolayer MoS_2-based sensor, highest imaging sensitivity of ~484 RIU^{-1} is obtained with Al thickness around 42.5 nm at λ = 785 nm, ~747 RIU^{-1} with Al thickness ~ 37.5 nm for λ = 1150 nm, and ~ 974 RIU^{-1} with Al thickness ~ 33.5 nm at wavelength λ = 1540 nm. This indicates that the proposed sensor not only protects the Al from oxidation, but also provides ultrahigh imaging sensitivities. It can be seen from Fig. 5 that the designed sensor shows significantly high imaging sensitivity for few MoS_2 layers with 35-50 nm Al thickness at wavelength λ = 785 nm, 30-45 nm Al thickness at λ = 1150 nm, and 25-45 nm Al thickness at λ = 1540 nm. It is noted that the proposed sensor with 15 layers MoS_2 at λ = 1150 nm can still exhibits sensitivity of more than 300 RIU^{-1} with Al thickness around 35 nm. Even for Al film coated with 30 MoS_2 layers, the proposed sensor can provide an imaging sensitivity of ~300 RIU^{-1} (more than 290 RIU^{-1}) at wavelength λ = 1540 nm with Al thickness around 30 nm.

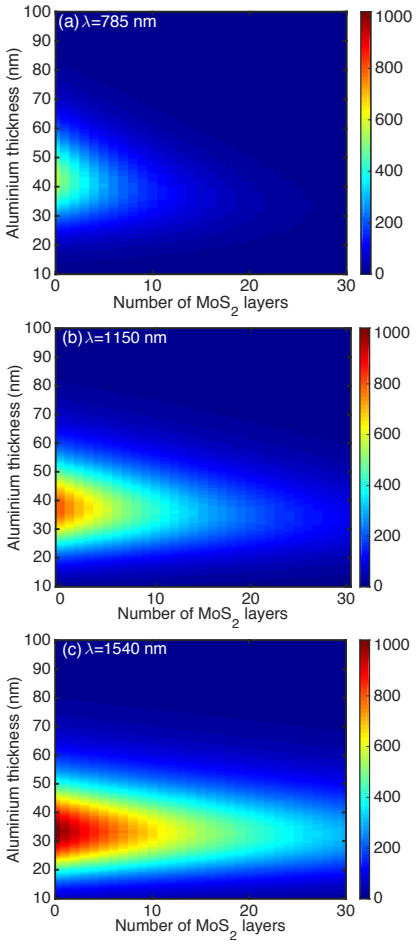


Fig. 5. Imaging sensitivity as a function of the number of MoS_2 layers and Al thickness at (a) λ = 785 nm, (b) λ = 1150 nm and (c) λ = 1540 nm.

The sensing layer RI is another important parameter for the sensor performance. As shown in Fig. 6(a), the resonance angle increases with the sensing layer RI, which can be understand from

the SPR resonance condition [2]:

$$\frac{2\pi}{\lambda} n_p \sin\theta_{\mathrm{SPR}} = \mathrm{Re}\left\{\frac{2\pi}{\lambda}\left(\frac{\epsilon_m n_s^2}{\epsilon_m + n_s^2}\right)^{1/2}\right\}, \tag{9}$$

where n_p is the RI of prism, ϵ_m is the dielectric constant of metal film. The left-hand side of Eq. (9) is the propagation constant of the incident light, and the term on the right hand side is the real part of propagation constant of SPW. The propagation constant of the SPW increases with the RI of sensing layer, which leads to the increase in the resonance angle. In addition, the resonance angle also increases with the incident wavelength (Fig. 6(a)). For the sensor performance, the FWHM increases and the imaging sensitivity decreases with the sensing layer RI (see Fig. 6(b) and (c)).

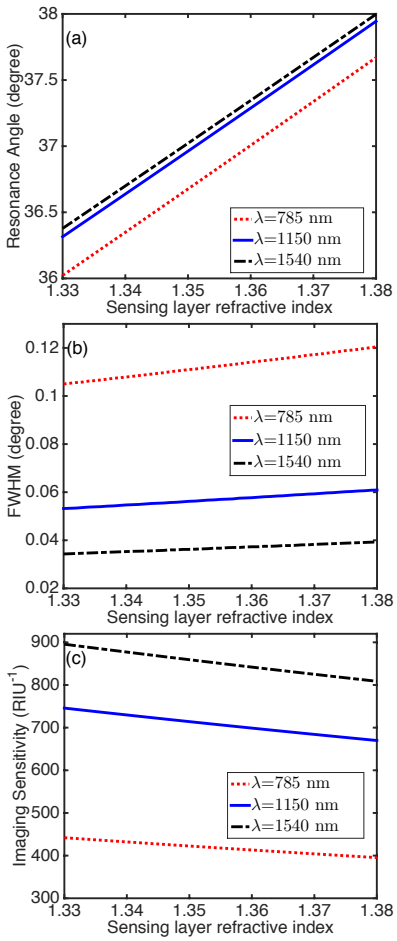


Fig. 6. (a) Resonance angle, (b) FWHM, and (c) imaging sensitivity as a function of the sensing layer refractive index at three different wavelengths, λ = 785 nm, 1150nm and 1540 for monolayer MoS_2 based imaging sensor. The Al thickness is 38 nm.

Other 2D TMDC materials, like Molybdenum diselenide ($MoSe_2$), Tungsten disulfide (WS_2) and Tungsten diselenide (WSe_2), have been proposed and demonstrated for sensing applications [23, 24, 37, 38]. It is interesting to compare the sensor performance of SPR imaging sensor with different TMDC materials. Here, we compare the imaging sensitivity and FWHM for SPR

imaging sensor with four TMDC materials (MoS_2, $MoSe_2$, WS_2, and WSe_2) at three different wavelengths, as shown in Fig. 7 and 8, respectively. The thickness of Al film are taken from Fig. 3 that have been optimized for the three wavelengths: 42.8 nm for λ = 785 nm, 37.6 nm for λ = 1150 nm and 33.4 nm for λ = 1540 nm. Similar to the MoS_2-based SPR imaging sensor, imaging sensitivity decreases while FWHM increases with the number of layers for $MoSe_2$-, WS_2-, and WSe_2-based imaging sensor. For λ = 785 nm, WSe_2 exhibits the highest imaging sensitivity with minimum FWHM, whereas $MoSe_2$-based sensor has the smallest sensitivity and maximum FWHM. At λ = 1150 nm, MoS_2 SPR imaging sensor has the maximum sensitivity as well as the minimum FWHM, same as the case of λ = 1540 nm. For the other three TMDC materials at wavelengths λ = 1150 nm and λ = 1540 nm, they exhibit similar imaging sensitivity, and WS_2-based SPR imaging sensor has the maximum FWHM. Therefore, to obtain a high performance SPR imaging sensor, one can choose WSe_2-based sensor at λ = 785 nm, while for wavelengths λ = 1150 nm and λ = 1540 nm, MoS_2 is a better choice.

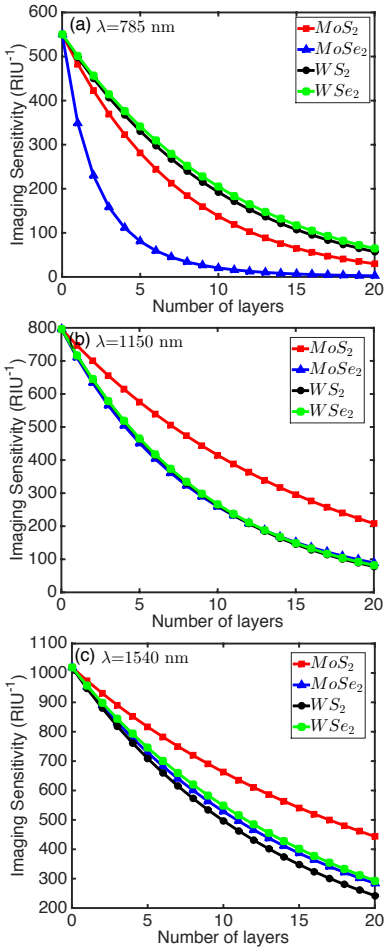


Fig. 7. Imaging sensitivity for SPR imaging sensor with multiple TMDC layers. (a) λ = 785 nm with 42.8 nm thick Al film, (b) λ = 1150 nm with 37.6 nm thick Al film, and (c) λ = 1540 nm with 33.4 nm thick Al film.

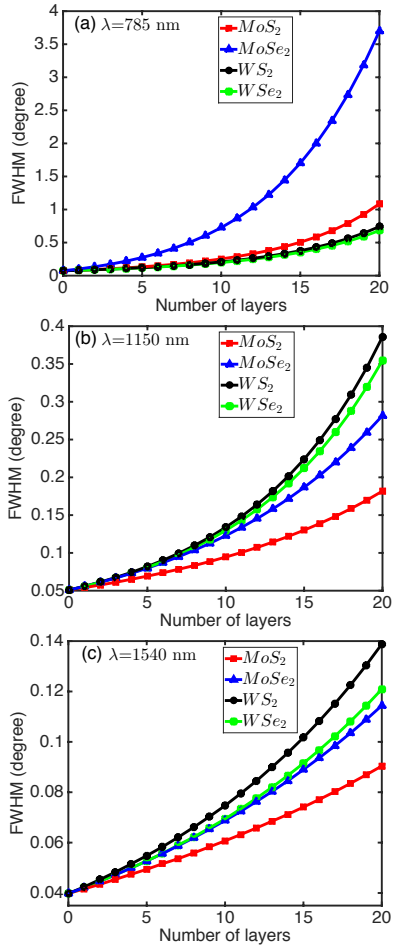


Fig. 8. FWHM for SPR imaging sensor with multiple TMDC layers. (a) λ = 785 nm with 42.8 nm thick Al film, (b) λ = 1150 nm with 37.6 nm thick Al film, and (c) λ = 1540 nm with 33.4 nm thick Al film.

4. Conclusion

In this work, an ultrahigh sensitive SPR imaging biosensor based on MoS_2-on-Al is proposed. In the designed biosensor structure, MoS_2 layers are employed to inhibit the oxidation of Al thin film and as the recognition layer to capture biomolecules. Graphene-on-Al based sensor exhibits better sensor performance than that of the proposed sensor in the visible range, however, the MoS_2-based SPR imaging biosensor overtakes its graphene counterparts in the near-infrared regime. It is found that the imaging sensitivity decreases with the number of MoS_2 layers applied, while the FWHM increases. A similar trend is observed with the RI of sensing layer. In addition, better sensor performance can be obtained at higher wavelength, where the imaging sensitivity can be as high as ~974 RIU^{-1} at wavelength λ = 1540 nm. Compared with other TMDC materials ($MoSe_2$, WS_2, and WSe_2) based biosensor, biosensor based on WSe_2 shows the best sensor performance at wavelength λ = 785 nm, while MoS_2-based biosensor has better performance than the other three biosensors at wavelengths λ = 1150 nm and λ = 1540 nm. We believe that the present study will be helpful in designing a high performance SPR imaging sensor for chemical and and biosensing applications.

Funding

Singapore ASTAR AME IRG (A1783c0011).